



Contents lists available at ScienceDirect



# Catalysis Today

journal homepage: [www.elsevier.com/locate/cattod](http://www.elsevier.com/locate/cattod)

## Mesoporous Nb<sub>2</sub>O<sub>5</sub> as solid acid catalyst for dehydration of D-xylose into furfural

C. García-Sancho, J.M. Rubio-Caballero, J.M. Mérida-Robles, R. Moreno-Tost,  
J. Santamaría-González, P. Maireles-Torres\*

Universidad de Málaga, Departamento de Química Inorgánica, Cristalografía y Mineralogía (Unidad Asociada al ICP-CSIC), Facultad de Ciencias, Campus de Teatinos, 29071 Málaga, Spain

### ARTICLE INFO

#### Article history:

Received 17 November 2013

Received in revised form 22 January 2014

Accepted 8 February 2014

Available online xxx

#### Keywords:

Mesoporous Nb<sub>2</sub>O<sub>5</sub>

Xylose dehydration

Biomass

Acid catalysis

### ABSTRACT

The acid-catalyzed dehydration of D-xylose to furfural has been investigated in a biphasic water-toluene system, using a mesoporous Nb<sub>2</sub>O<sub>5</sub> catalyst prepared by a neutral templating route. The catalytic behavior was compared with a commercial Nb<sub>2</sub>O<sub>5</sub>. Materials were characterized by XRD, XPS, TEM, NH<sub>3</sub>-TPD, Raman spectroscopy and N<sub>2</sub> sorption. The D-xylose conversion and furfural yield over the mesoporous niobia were found to increase with reaction temperature and time, in such a way that at 170 °C and 90 min, a D-xylose conversion and a furfural yield were higher than 90% and 50%, respectively. However, the commercial crystalline niobia displayed a low activity. The stability of the mesoporous catalyst has been demonstrated by XRD and N<sub>2</sub> sorption, and corroborated by the absence of significant niobium leaching in solution.

© 2014 Elsevier B.V. All rights reserved.

### 1. Introduction

Recent years have witnessed increasing interest in the development of catalytic processes for biomass conversion, as an alternative feedstock to crude oil, for the production of renewable chemicals and biofuels in biorefineries. In these facilities, biomass is converted into power, heat, biofuels and value-added chemicals, by using integrated processes. In this context, monosaccharides present in cellulose, hemicelluloses and starch, obtained from biomass via deconstruction, can be used as raw materials to produce a large variety of high value-added chemicals, with many industrial applications [1–3]. Particularly, xylose, a C5 sugar, can be chemically transformed into important products, such as furfural, furfuryl alcohol, ethanol, xylitol, 2-methylfuran and 2-methyltetrahydrofuran, amongst others [4–6]. Furfural has been identified as one of the most important platform molecules for the production of chemicals and biofuels, which are very important for the design of biorefining strategies [7,8].

The use of solid acid catalysts for the dehydration of xylose into furfural has demonstrated to be a promising alternative to the conventional homogeneous process using sulphuric acid, which is toxic, corrosive and suffers from several drawbacks common

to homogeneous catalysts [5,3,9]. Many types of solid acid catalysts have been tested for the dehydration of xylose to furfural, such as zeolites [10], exfoliated titanate, niobate and titanoniobate nanosheets [11], sulfated metal oxides [12,13], sulfonic acid-modified mesoporous silica [14], exchange resins [15], micro-porous silicoaluminophosphates [16], mesoporous silica-alumina [17], bulk cesium salts of 12-tungstophosphoric acid or supported on MCM-41 [18], sulfonated graphene oxide [19] and metal phosphates and pyrophosphates [20–22].

On the other hand, much attention has been paid to the tuning of the surface and textural properties of mesoporous materials, originating active and selective catalysts and catalyst supports for many different catalytic processes. In this sense, the synthesis of mesoporous transition metal oxides has allowed to provide highly active solid acid catalysts [23–29]. Likewise, bulk niobic acid (Nb<sub>2</sub>O<sub>5</sub>·nH<sub>2</sub>O) is known as a water-tolerant solid acid that exhibits catalytic activity in hydrated form after being calcined at 100–300 °C [30,31]. A wide range of methodological approaches has been reported to synthesize mesoporous niobium oxide [32–36]; thus, a niobium oxide with highly ordered 3D mesoporous structure has been prepared via a neutral templating route, with addition of a trace amount of cations [37,38].

In the present work, the dehydration of xylose to furfural has been studied over a mesoporous niobium oxide catalyst, using a biphasic water-toluene solvent system, at different reaction temperatures. This material could be considered suitable for this

\* Corresponding author. Tel.: +34 952137534; fax: +34 952131870.

E-mail address: [maireles@uma.es](mailto:maireles@uma.es) (P. Maireles-Torres).

reaction due to its large pore diameter, water-tolerance and acidic properties. The catalytic behavior is compared with that of a commercial niobium oxide to establish the effect of the textural properties on the catalytic performance.

## 2. Experimental

### 2.1. Catalyst preparation

The synthesis of a mesoporous niobium oxide was carried out by using a neutral templating route, as previously reported by Lee et al. [37]. Briefly, 7 mmol of  $\text{NbCl}_5$  were added to a template solution formed by 0.22 mmol of P-L121 (triblock copolymer ( $\text{C}_3\text{H}_6\text{O}\cdot\text{C}_2\text{H}_4\text{O}_x$ ) in 10 g of n-propanol. After vigorous stirring for 5 min, 1.0 mL of a 0.05 M NaCl aqueous solution was added, and the resulting solution was stirred for 30 min at room temperature. The Nb:P-L121:n-propanol:NaCl:H<sub>2</sub>O molar ratio was 35:1:835:0.25:280. The solution was aged at 40 °C for one week. The structure-directing agent was removed by calcination in air (5 h) at two different temperatures: 450 and 550 °C. Thus, the catalysts were labeled as Nb\_450 and Nb\_550, where the number indicates the calcinations temperature. Commercial  $\text{Nb}_2\text{O}_5$ , purchased from Aldrich, was used for comparison (Nb\_C).

### 2.2. Catalyst characterization

Several characterization techniques were employed to evaluate the physico-chemical properties of the mesoporous niobium oxide. Elemental analysis was performed on a LECO CHNS-932 micro-analyzer. Powder X-ray diffraction (XRD) measurements were performed on a Philips X'Pert PRO MPD automated diffractometer, over a  $2\theta$  range with Bragg-Brentano geometry using the Cu K $\alpha$  radiation and a graphite monochromator. The scans covered the  $2\theta$  range from 1° to 70°.

$\text{N}_2$  adsorption-desorption isotherms at –196 °C of calcined materials were obtained using an ASAP 2020 model of gas adsorption analyzer from Micromeritics, Inc. Prior to  $\text{N}_2$  adsorption, the samples were evacuated at 200 °C and  $1 \times 10^{-2}$  Pa for 10 h. The Barrett-Joyner-Halenda method (BJH) was used to determine the pore size distribution.

The morphology of the mesostructured solid was studied by transmission electron microscopy (TEM), by using a Philips CM 200 Supertwin-DX4 microscope. The sample was dispersed in ethanol, and a drop of the suspension was put on a Cu grid (300 mesh).

Temperature-programmed desorption of ammonia ( $\text{NH}_3$ -TPD) was carried out to evaluate the total acidity of the catalyst. The material was pre-treated under a helium flow at 100 °C, and then ammonia was adsorbed at the same temperature. The analysis of the desorbed ammonia was performed up to 500 °C, with a heating rate of 10 °C min<sup>−1</sup> by using helium as carrier gas. The evolved ammonia was analyzed using a TCD detector of a gas chromatograph (Shimadzu GC-14A).

X-ray photoelectron spectroscopy (XPS) studies were performed with a Physical Electronics PHI 5700 spectrometer equipped with a hemispherical electron analyzer (model 80-365B) and a Mg K $\alpha$  (1253.6 eV) X-ray source. High-resolution spectra were recorded at 45° take-off-angle by a concentric hemispherical analyzer operating in the constant pass energy mode at 29.35 eV, using a 720  $\mu\text{m}$  diameter analysis area. Charge referencing was done against adventitious carbon (C 1s at 284.8 eV). The pressure in the analysis chamber was kept lower than  $5 \times 10^{-6}$  Pa. PHI ACCESS ESCA-V6.0 F software package was used for data acquisition and analysis. A Shirley-type background was subtracted from the signals. Recorded spectra were always fitted using Gauss-Lorentz

curves in order to determinate more accurately the binding energy of the different element core levels.

Raman spectra were recorded on a Raman Senterra (Bruker) microspectrometer equipped with a thermoelectrically cooled charge coupled device (CCD) detector. A Nd:YAG laser was used as the excitation source at 532 nm and the laser power was set to 2 mW. Raman spectroscopy was performed on powder samples without any previous treatment.

### 2.3. Catalytic reaction

Catalytic experiments were performed in batch, by using a glass pressure tube with thread bushing (Ace, 15 mL, pressure rated to 10 bar) and magnetic stirring. In a typical procedure, 150 mg of D-xylose (SigmaUltra, >99%), 50 mg of catalyst, deionized water (1.5 mL) and toluene (3.5 mL, Sigma-Aldrich, >99.5%) were poured into the reactor. Prior the experiments, reactors were always purged with nitrogen. The reaction mixture was heated with a thermostatically controlled oil bath and stirred magnetically at 600 rpm. After reaction time, the reaction was quenched by submerging the reactor in a water bath cooled with ice; the liquid phases were separated, filtered and the analysis of products was performed in both phases by high performance liquid chromatography (HPLC). A JASCO instrument equipped with quaternary gradient pump (PU-2089), multiwavelength detector (MD-2015), autosampler (AS-2055), column oven (co-2065) using a PHENOMENEX LUNA C18 reversed-phase column (250 mm × 4.6 mm, 5  $\mu\text{m}$ ) and PHENOMENEX REZEX RHM-Monosaccharide H+(8%)C18 (300 mm × 7.8 mm, 5  $\mu\text{m}$ ) was employed. The disappearance of xylose was monitored using a refractive index detector, while furfural production was monitored using a UV detector. The mobile phases consisted in pure methanol (flow rate 0.5 mL min<sup>−1</sup>) for Luna C18 and 0.005 M H<sub>2</sub>SO<sub>4</sub> aqueous solution (flow rate 0.4 mL min<sup>−1</sup>) for Rezex RHM-Monosaccharide column, being the column at room temperature and 80 °C, respectively.

## 3. Results and discussion

### 3.1. Catalytic characterization

X-ray diffraction was used to corroborate the mesostructured character of the material obtained after calcination to remove the structure-directing agent, once the hybrid organo-inorganic structure has been formed. The XRD pattern in the low angle region showed the characteristic intense and broad reflection of mesostructured solids, at around  $2\theta = 1.5^\circ$  (Fig. 1), which can be indexed to the d<sub>100</sub> diffraction signal (6.2 nm), as previously reported by Lee et al. [37]. However, higher order peaks were not observed, thus pointing out the lack of long-range order of the hexagonal mesostructure of niobium oxide. The amorphous nature of the pore walls of the synthesized niobia can be inferred from the absence of diffraction peaks in the high angle region. The effective removing of the organic moieties after calcination at 450 °C was confirmed by CHN analysis, which gave percentages of carbon and hydrogen of 0.07 and 0.38%, respectively.

However, the thermal treatment of the mesostructured niobia at higher temperature (550 °C) provoked the destruction of the mesoporous structure, since the low-angle diffraction peak disappeared and, concomitantly, new diffraction peaks of low intensity appeared in the high angle region, which were associated to the orthorhombic phase of  $\text{Nb}_2\text{O}_5$ . In this sense, Braga et al. [38] previously reported that calcination temperatures lower than 450 °C generated an amorphous  $\text{Nb}_2\text{O}_5$  phase, but the orthorhombic niobia crystallized at increasing calcination temperature. On the other hand, as expected, the XRD pattern of commercial niobia

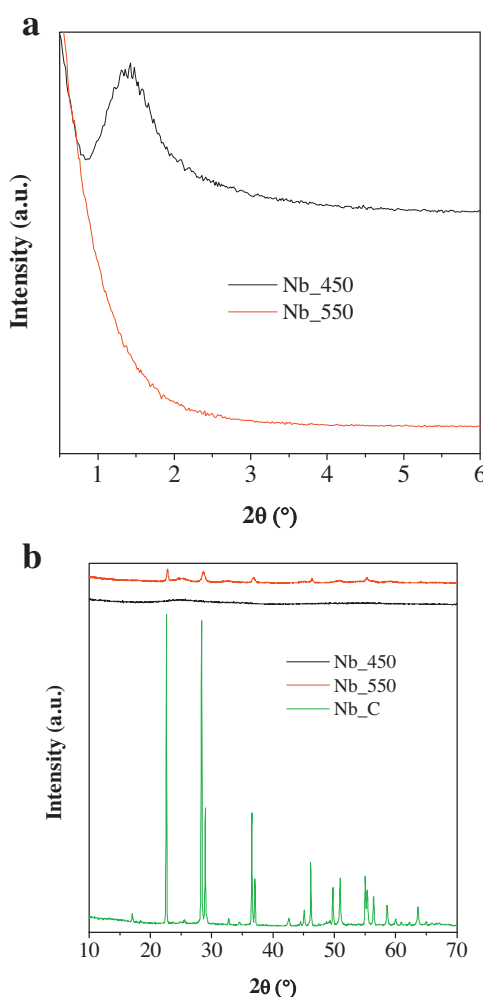


**Fig. 1.** Low-angle (a) and high-angle (b) XRD patterns of  $\text{Nb}_2\text{O}_5$  samples.

consisted in intense and narrow diffraction peaks associated to this orthorhombic crystalline phase.

The structural features associated to the lack of long-range order and the amorphous walls were confirmed by transmission electron microscopy (TEM), where a wormhole-like mesoporous structure was observed in the corresponding micrograph (Fig. 2). Moreover, the pore sizes deduced from the micrographs were rather uniform and around 4–6 nm in size.

Table 1 summarizes the textural parameters of the mesoporous material and the commercial niobia. The Nb\_450 sample showed a  $\text{N}_2$  adsorption–desorption isotherm of Type IV, according to the IUPAC classification, typical of mesoporous materials (Fig. 3a). The BJH analysis, used to elucidate the pore size distribution, revealed the presence of uniform-sized mesopores with an average diameter of 3.9 nm (Fig. 3b). The BET surface area and pore volume values were  $123 \text{ m}^2 \text{ g}^{-1}$  and  $0.152 \text{ cm}^3 \text{ g}^{-1}$ , respectively. However,

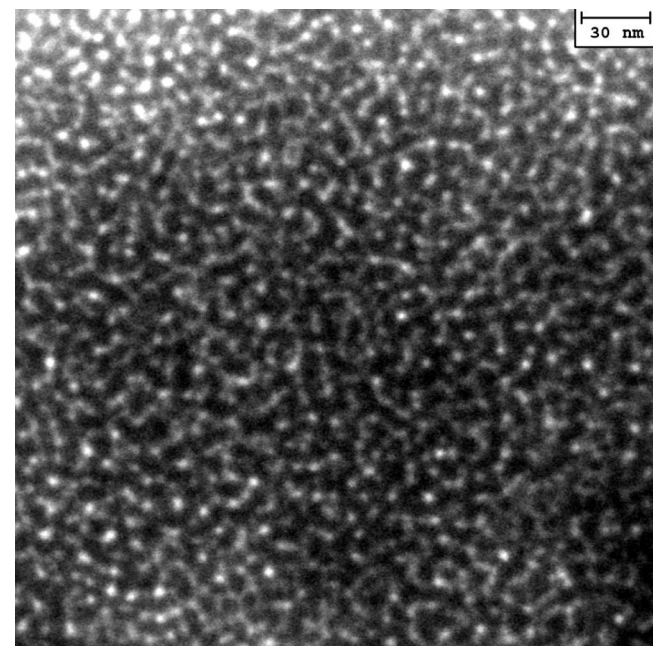


**Fig. 2.** TEM image of Nb\_450.

commercial niobia possessed a very low BET surface area ( $4 \text{ m}^2 \text{ g}^{-1}$ ), being mainly associated to the external surface of crystallites.

XPS analysis is a powerful tool to characterize the chemical state of the surface of catalysts. Thus, the chemical state of Nb can be inferred from the binding energy (BE) of the corresponding photoelectronic peak. The XPS data are summarized in Table 2. The two components of the Nb 3d doublet could be well resolved at 206.8–207.0 eV ( $3\text{d}_{5/2}$ ) and 209.6–209.7 eV ( $3\text{d}_{3/2}$ ), being these values typical of Nb(V) in an oxidic environment (Fig. 4a). On the other hand, the O 1s region only showed a single and almost symmetric peak at 530.2 eV for both commercial and mesoporous  $\text{Nb}_2\text{O}_5$  (Fig. 4b).

It is well known that dehydration of D-xylose is an acid-catalyzed process which depends on the amount and type of acid sites present on the surface of the solid catalyst. For this reason, the total acidity of the mesoporous niobia was evaluated by  $\text{NH}_3$ -TPD. The total amount of desorbed  $\text{NH}_3$  was  $198.6 \mu\text{mol g}^{-1}$ . Moreover, the integration of the  $\text{NH}_3$ -TPD curve revealed the presence of acid sites with a wide range of strength, which can be explained by the existence of different niobia environments on the surface of the amorphous walls of mesoporous niobia. However, the Nb\_C sample did not adsorb any ammonia, since no desorption was detected by means of  $\text{NH}_3$ -TPD.

Raman spectroscopy has been also used to study the nature of the mesoporous niobium oxide. The FT-Raman spectrum (Fig. 5) displayed a broad band in the  $500$ – $750 \text{ cm}^{-1}$  region, which may be associated to slightly distorted octahedral  $\text{NbO}_6$  structures. Other vibration bands were found between  $100$  and  $350 \text{ cm}^{-1}$ , which

**Table 1**  
Textural data and acidic properties.

Catalyst	$S_{\text{BET}}$ ( $\text{m}^2 \text{ g}^{-1}$ )	$V_p$ ( $\text{cm}^3 \text{ g}^{-1}$ )	Average $d_p$ (nm)	$\mu\text{mol NH}_3$ $\text{g}_{\text{cat}}^{-1}$	$\mu\text{mol NH}_3 \text{ m}^{-2}$
Nb_450	123	0.152	3.9	198.6	1.61
Nb_550	48	0.219	14.5	96.5	0.5
Nb_C <sup>a</sup>	4	0.013	20.7	–	–

<sup>a</sup> The acidity of the Nb\_C cannot be determined by means of TPD-NH<sub>3</sub>.

**Table 2**  
XPS data of niobium oxides.

Catalyst	Binding energy (eV)		Atomic concentration			
	$\text{Nb } 3\text{d}_{5/2}$	O 1s	C 1s	Nb 3d	O 1s	O/Nb
Nb_450 (fresh)	207.0	530.3	21.5	23.6	54.9	2.3
Nb_450 (spent)	207.0	530.2	30.7	18.6	50.7	2.7
Nb_C (fresh)	207.0	530.1	27.0	21.6	51.4	2.4

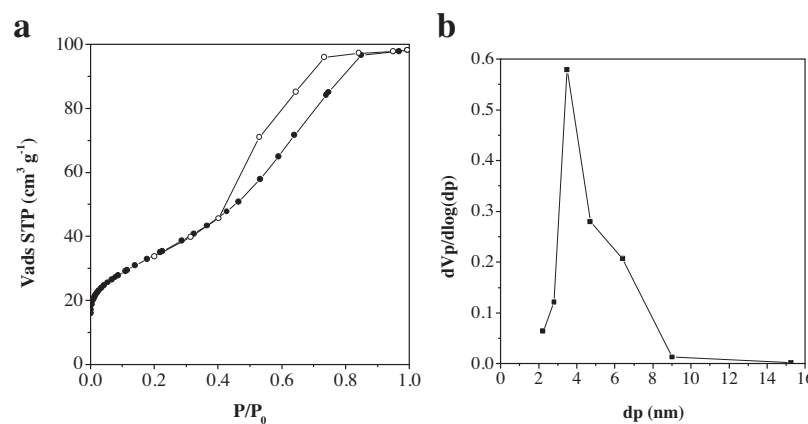


**Fig. 3.** (a)  $\text{N}_2$  adsorption–desorption isotherms and (b) pore size distribution of Nb\_450 sample.

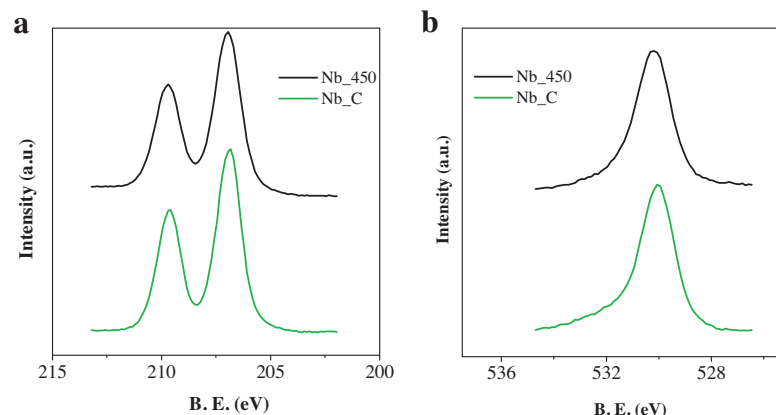


**Fig. 4.** X-ray photoelectronic spectra of the Nb 3d (a) and O 1s (b) regions.

corresponds to the symmetric stretching mode of niobia polyhedral and the bending modes of Nb–O–Nb linkages. These different environments agree well with the results obtained from  $\text{NH}_3$ -TPD data, where the presence of a broad distribution of acid strengths was deduced.

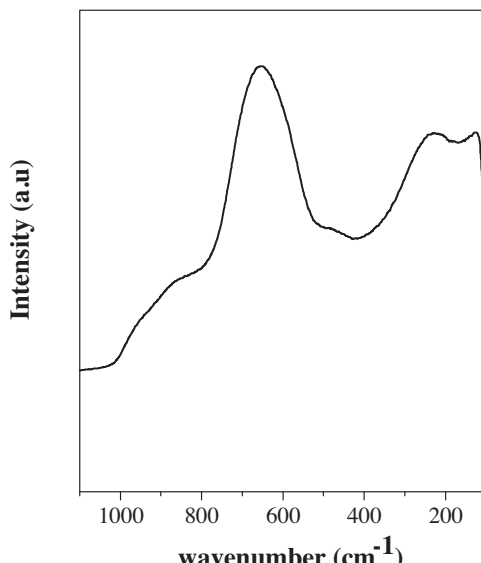


**Fig. 5.** Raman spectra of Nb\_450.

### 3.2. Catalytic results

One of the main drawbacks in the synthesis of furfural from xylose over solid acid catalysts is the formation of humins, which are carbonaceous species produced from furfural and reaction intermediates, mainly in aqueous media. This fact gives rise to a decrease of the furfural yield, and the deactivation of solid catalysts. Several studies have suggested different ways to inhibit the formation of humins, being the selective extraction of furfural from the aqueous solution by using an immiscible organic phase, in a biphasic system, an interesting alternative. This technique has been reported to be the most promising in terms of yield and flexibility [39]. Thus, Dumesic et al. [40,41] obtained high yields of 5-hydroxymethylfurfural from hexoses by using biphasic systems.

In the present catalytic study, a biphasic water–toluene system was used to evaluate the dehydration of xylose to furfural, by taking advantage of the high solubility of xylose in water and its low solubility in toluene, whereas furfural is distributed in the two liquid phases with a partition ratio ((mol of furfural in toluene)/(mol of furfural in water)) in the range of 8–10, at room temperature. This reaction system helps to minimize secondary reactions, which are responsible of humins formation, thus ameliorating the furfural yield.

Firstly, the influence of the reaction temperature on the catalytic performance was studied in the range 140–170 °C. Kinetic profiles at different reaction temperatures evidenced that xylose conversion and furfural yield increased with reaction temperature and time (Fig. 6). Thus, at 170 °C, xylose conversions higher than 90% were attained after only 30 min, with furfural yields higher than

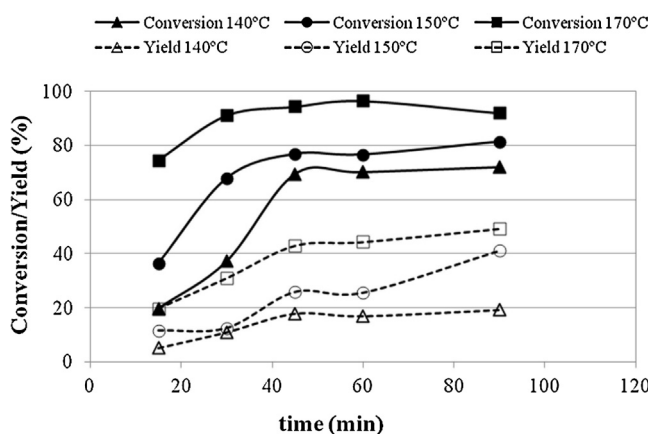


**Fig. 6.** Xylose conversion and furfural yield as function of temperature and time on stream for Nb.450 catalyst, with a xylose:catalyst weight ratio of 3.

30%, which increased until 53.5% at 90 min. However, it is noteworthy that a high furfural yield (41.1%) was already achieved at 150 °C, with a similar reaction time. It can be observed that the xylose conversion and furfural yield values were barely improved after 45 min of reaction, mainly at 170 °C. Under similar experimental conditions, a niobia supported on mesoporous MCM-41 silica attained a conversion of 74.5% and a furfural yield of 36.5% at 170 °C, but after 180 min [42]. However, furfural yield attained a value of 60% after addition of NaCl in the reaction medium. Although similar xylose conversion and furfural yield were obtained with phosphates based catalysts [20–22], the mesoporous niobium oxide required a shorter time to attain them at the same reaction temperature and even close values were achieved at 150 °C. Also, this catalyst demonstrated a high stability considering that leaching was negligible (vide infra), whereas water-soluble species were found for the vanadyl pyrophosphate [22].

There are different strategies to increase the number of acid sites associated to niobia, being the most usual synthetic approach its incorporation, either by impregnation or in the synthesis step, on a support with a high specific surface area [42–45]. These supported niobia catalysts, as previously indicated, have been already used in the dehydration of xylose to furfural [42,45]. The present results demonstrate that the synthesis of a mesostructured form of niobia is another feasible strategy to prepare very active catalysts for xylose dehydration.

By considering the catalytic behavior of mesoporous niobia as a function of reaction time and temperature, the evaluation of other reaction parameters has been carried out at 150 °C and 45 min. The influence of the catalyst concentration on the catalytic reaction was studied by varying the xylose:catalyst weight ratio from 4:1 to 1:1, in a biphasic H<sub>2</sub>O/toluene system. The xylose conversion increased monotonously with the xylose:catalyst ratio, reaching a maximum value of 0.084 mmol xylose converted per g<sub>cat</sub> and h, for a ratio of 4:1. However, the yield of furfural decreased in comparison with a 3:1 ratio (Fig. 7). This fact could be explained by the existence of secondary reactions, which are favored in excess of furfural, thus decreasing its yield.

The catalytic behavior of the mesoporous Nb<sub>2</sub>O<sub>5</sub> catalyst was compared with that of a commercial Nb<sub>2</sub>O<sub>5</sub>. Moreover, the dehydration reaction was performed in the absence of catalyst, under the same experimental conditions (150 °C and 45 min), in order to assess the contribution of the thermal process to the overall catalytic activity (Fig. 8). The conversion of xylose in the non-catalyzed process was practically negligible, and the catalytic performance of the commercial Nb<sub>2</sub>O<sub>5</sub> gave rise to low xylose conversion (22.3%) and furfural yield (3.4%). Therefore, the textural properties have a strong influence on the catalytic activity, since the mesoporous

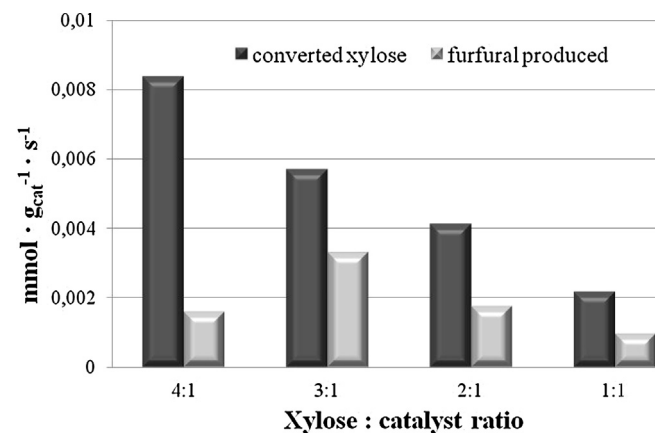


**Fig. 7.** Xylose conversion and furfural yield as function of xylose:catalyst weight ratio for the Nb.450 catalyst, at 150 °C and 45 min.

structure facilitates the accessibility of xylose molecules to the acid sites located in the pores. Concerning the nature of these acid sites, both Lewis and Brønsted acid sites are active in the dehydration of xylose; however, Lewis acid sites provide higher activities but furfural selectivity usually is less [46]. It has also been demonstrated that the Lewis acid sites promote a faster xylose dehydration rate to yield a xylulose isomer, which requires Brønsted sites to be further dehydrated to furfural [47,48]. It is well known that niobia exhibits Lewis acid sites associated to Nb species deficiently coordinated, but the presence of water can convert Nb–O–Nb linkages in Brønsted acid sites. Therefore, the fast kinetic of the catalytic process by using this mesoporous niobia may be associated to its Lewis acidity, being furfural selectivity based on its Brønsted acid sites, which were generated by interaction of surface Lewis acid sites of niobia with water molecules at the reaction temperature. The large pore diameter favors the diffusion of reactants and products to/from the active sites located on the pore surface of mesoporous niobia, whereas in the case of crystalline niobia, the catalytic sites are on the external surface of crystallites. Besides, by using the mesoporous niobia, after calcination at 550 °C, with a lower specific surface area (48 m<sup>2</sup> g<sup>-1</sup>) and acid sites density (0.50 μmol NH<sub>3</sub> desorbed m<sup>-2</sup>) (Table 1), despite having even a larger average pore size (14.5 nm), the catalytic activity is reduced.

On the other hand, Dias et al. reported the loss of structural ordering and leaching of the niobium species in the study of the catalytic dehydration of xylose over microporous and mesoporous niobium silicates [45]. In the present study, the leaching of niobium from the solid catalyst was evaluated by analyzing its presence

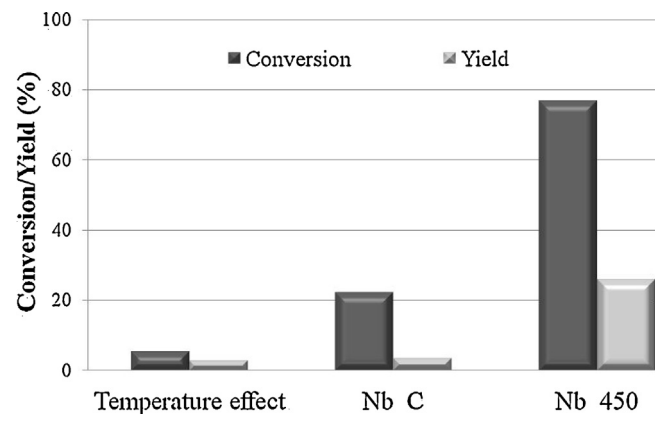


**Fig. 8.** Xylose conversion and furfural yield for non-catalytic process, commercial Nb<sub>2</sub>O<sub>5</sub> and the Nb.450 catalyst, at 150 °C and 45 min, with a xylose:catalyst weight ratio of 3:1.

in both phases, water and toluene, by using inductively coupled plasma-mass spectrometry (ICP-MS). The total amount of niobium in solution was lower than 0.5 wt% of the niobium initially present in the solid catalyst, thus demonstrating the stability of this acid solid catalyst.

Finally, the spent mesoporous niobia, after reaction at 150 °C for 45 min, was studied by different characterization techniques. In this sense, N<sub>2</sub> sorption at -196 °C demonstrated that the BET surface area was barely affected by the catalytic process, as can be inferred from the value of 114 m<sup>2</sup> g<sup>-1</sup>. The O 1s and Nb 3d signals deduced from X-ray photoelectron spectroscopy are weak, which can be attributed to the presence of a large amount of carbonaceous deposits on the catalyst surface; however, no significant differences in the BE or XPS atomic ratios were observed between the fresh and spent catalysts. The surface O/Nb atomic ratios (Table 2) were very close, although the high value (2.7) detected for the spent catalyst could be explained by the presence of humins on the external catalyst surface, which are responsible of the loss of furfural yield. This is confirmed by CHN analysis, with percentages of C and H are 4.11 and 0.76%.

#### 4. Conclusions

The synthesis of mesoporous niobia, in the presence of a neutral structure directing agent and subsequent calcination, is an alternative method to generate a high amount of surface niobia species. The acid-catalyzed dehydration of D-xylose to furfural was investigated over this mesoporous niobia, and the catalytic behavior was compared with that of a commercial Nb<sub>2</sub>O<sub>5</sub>. Its physico-chemical characterization has demonstrated the existence of mesopores of 3.9 nm of average diameter, and an acidity of 198.6 μmol g<sup>-1</sup>. The D-xylose conversion and furfural yield were found to increase with reaction temperature and time, in such a way that at 170 °C and 90 min, a conversion higher than 90% and a furfural yield of 50% were achieved. The stability of this catalyst has been demonstrated because no significant niobium leaching has been observed.

#### Acknowledgments

The authors are grateful to financial support from the Spanish Ministry of Economy and Competitiveness (CTQ2012-38204-C03-02 project), Junta de Andalucía (P09-FQM-5070) and FEDER funds. RMT would like to thank this Ministry of Science and Innovation for the financial support under the Program Ramon y Cajal (RYC-2008-03387).

#### References

- [1] A. Corma, S. Iborra, A. Velty, *Chem. Rev.* 107 (2007) 2411–2502.
- [2] P. Gallezot, *Chem. Soc. Rev.* 41 (2012) 1538–1558.
- [3] M.J. Climent, A. Corma, S. Iborra, *Green Chem.* 13 (2011) 520–540.
- [4] J.P. Lange, E. van der Heide, J. van Buijtenen, R. Price, *ChemSusChem* 5 (2012) 150–166.

- [5] R. Karinen, K. Vilonen, M. Niemela, *ChemSusChem* 4 (2011) 1002–1016.
- [6] S.G. Wettstein, D. Martín-Alonso, E.I. Gürbüz, J.A. Dumesic, *Curr. Opin. Chem. Eng.* 1 (2012) 218–224.
- [7] T. Werpy, G. Petersen (Eds.), *Top Value Added Chemicals from Biomass. Results of Screening for Potential Candidates from Sugars and Synthesis Gas*, vol. 1, Report No. DOE/GO-102004-1992, National Renewable Energy Laboratory, Golden, CO, 2004.
- [8] K.J. Zeitsch, *The Chemistry and Technology of Furfural and its Many By-Products*, vol. 13, 1st ed., Elsevier, The Netherlands, 2000 (Sugar Series).
- [9] S. Dutta, S. De, B. Saha, M.I. Alam, *Catal. Sci. Technol.* 2 (2012) 2025–2036.
- [10] J. Lessard, J.-F. Morin, J.-F. Wehrung, D. Magnin, E. Chorne, *Top. Catal.* 53 (2010) 1231–1234.
- [11] A.S. Dias, S. Lima, D. Carriazo, V. Rives, M. Pillinger, A.A. Valente, *J. Catal.* 244 (2006) 230–237.
- [12] A.S. Dias, S. Lima, M. Pillinger, A.A. Valente, *Catal. Lett.* 114 (2007) 151–160.
- [13] X. Shi, Y. Wu, P. Li, H. Yi, M. Yang, G. Wang, *Carbohydr. Res.* 346 (2011) 480–487.
- [14] I. Agirrezabal-Telleria, J. Requies, M.B. Gümez, P.L. Arias, *Appl. Catal. B* 115–116 (2012) 169–178.
- [15] I. Agirrezabal-Telleria, A. Larreategui, J. Requies, M.B. Gümez, P.L. Arias, *Biore-sour. Technol.* 102 (2011) 7478–7485.
- [16] S. Lima, A. Fernandes, M.M. Antunes, M. Pillinger, F. Ribeiro, A.A. Valente, *Catal. Lett.* 135 (2010) 41–47.
- [17] J. Zhang, J. Zhuang, L. Lin, S. Liu, Z. Zhang, *Biomass Bioenergy* 39 (2012) 73–77.
- [18] A.S. Dias, S. Lima, M. Pillinger, A.A. Valente, *Carbohydr. Res.* 341 (2006) 2946–2953.
- [19] E. Lam, J.H. Chong, E. Majid, Y. Liu, S. Hrapovic, A.C.W. Leung, J.H.T. Luong, *Carbon* 50 (2012) 1033–1043.
- [20] L. Cheng, X. Guo, C. Song, G. Yu, Y. Cui, N. Xue, L. Peng, X. Guo, W. Ding, *RSC Adv.* 3 (2013) 23228–23235.
- [21] X.C. Li, Y. Zhang, Y.J. Xia, B.C. Hu, L. Zhong, Y.Q. Wang, G.Z. Lu, *Wuli Huaxue Xuebao/Acta Physico-Chimica Sinica* 28 (2012) 2349–2354.
- [22] I. Sádaba, S. Lima, A.A. Valente, M. López Granados, *Carbohydr. Res.* 346 (2011) 2785–2791.
- [23] Y.Y. Huang, T.J. McCarthy, W.M.H. Sachtler, *Appl. Catal. A* 148 (1996) 135.
- [24] M. Chidambaram, D. Curulla-Ferre, A.P. Singh, B.G. Anderson, *J. Catal.* 220 (2003) 442.
- [25] S.M. Landge, M. Chidambaram, A.P. Singh, *J. Mol. Catal. A* 213 (2004) 257.
- [26] C.-C. Hwang, C.Y. Mou, *J. Phys. Chem. C* 113 (2009) 5212.
- [27] Y. Rao, M. Trudeau, D. Antonelli, *J. Am. Chem. Soc.* 128 (2006) 13996.
- [28] Y. Rao, J. Kang, D. Antonelli, *J. Am. Chem. Soc.* 130 (2008) 394.
- [29] J. Kang, Y. Rao, M. Trudeau, D. Antonelli, *Angew. Chem. Int. Ed.* 47 (2008) 4896.
- [30] K. Tanabe, *Catal. Today* 78 (2003) 65.
- [31] I. Nowak, M. Ziolek, *Chem. Rev.* 99 (1999) 3603.
- [32] P. Yang, D. Zhao, D.I. Margolese, B.F. Chmelka, G.D. Stucky, *Nature* 396 (1998) 152.
- [33] P. Yang, D. Zhao, D.I. Margolese, B.F. Chmelka, G.D. Stucky, *Chem. Mater.* 11 (1999) 2813.
- [34] D.M. Antonelli, J.Y. Ying, *Angew. Chem. Int. Ed. Engl.* 35 (1996) 426.
- [35] D.M. Antonelli, A. Nakahira, J.Y. Ying, *Inorg. Chem.* 35 (1996) 3126.
- [36] T. Sun, J.Y. Ying, *Nature* 389 (1997) 704–706.
- [37] B. Lee, D. Lu, J.N. Kondo, K. Domen, *J. Am. Chem. Soc.* 124 (2002) 11256–11257.
- [38] V.S. Braga, J.A. Dias, S.C.L. Dias, J.L. de Macedo, *Chem. Mater.* 17 (17) (2005) 690–695.
- [39] D.G. Vlachos, S. Caratzoulas, *Chem. Eng. Sci.* 65 (2010) 18–29.
- [40] Y. Román-Leshkov, J.N. Chheda, J.A. Dumesic, *Science* 312 (2006) 1933–1937.
- [41] J.N. Chheda, Y. Román-Leshkov, J.A. Dumesic, *Green Chem.* 9 (2007) 342–350.
- [42] C. García-Sancho, I. Sádaba, R. Moreno-Tost, J. Mérida-Robles, J. Santamaría-González, M. López-Granados, P. Maireles-Torres, *ChemSusChem* 6 (2013) 635–642.
- [43] M. Ziolek, I. Nowak, J.C. Lavalle, *Catal. Lett.* 45 (1997) 259–265.
- [44] L. Zhang, J.Y. Ying, *AIChE J.* 43 (1997) 2793–2801.
- [45] A.S. Dias, S. Lima, P. Brandão, M. Pillinger, J. Rocha, A.A. Valente, *Catal. Lett.* 108 (2006) 179–186.
- [46] R. Weingarten, G. Tompsett, W. Conner, G. Huber, *J. Catal.* 279 (2011) 174–182.
- [47] V. Choudhary, A. Pinar, S. Sandler, D. Vlachos, R. Lobo, *ACS Catal.* 1 (2011) 1724–1728.
- [48] V. Choudhary, S. Sandler, D. Vlachos, *ACS Catal.* 2 (2012) 2022–2028.